Maximum Sum Rate of MCM-NOMA in Future Vehicular Sensor Networks

Alain Allouis, Anis Amazigh Hamza, Iyad Dayoub, Soumaya Cherkaoui

Sensor Applications

Maximum Sum Rate of MCM-NOMA in Future Vehicular Sensor Networks

Alain Allouis[1], Anis Amazigh Hamza[1*], Iyad Dayoub[1,2**], and Soumaya Cherkaoui[3**]

[1]*Univ. Polytechnique Hauts-de-France, CNRS, Univ. Lille, UMR 8520 - IEMN - Institut d'Electronique de Microélectronique et de Nanotechnologie, F-59313 Valenciennes, France*
[2]*INSA Hauts-de-France, F-59313 Valenciennes, France*
[3]*Department of Computer and Software Engineering, Polytechnique Montréal, Montréal, QC H3T 1J4, Canada*
[*] *Student Member, IEEE*
[**] *Senior Member, IEEE*

Manuscript received AAAA 00, 0000; revised AAAA 00, 0000; accepted AAAA 00, 0000. Date of publication AAAA 00, 0000; date of current version AAAA.

Abstract—This letter addresses the challenge of determining the maximum sum rate achievable in high mobility scenarios with time and frequency selectivity in 5G V2X communications, particularly in the context of IoT/sensor networks. We derive a closed-form expression for the maximum sum rate of a multicarrier non-orthogonal multiple access (NOMA) system with n users, and validate our theoretical results through simulations by comparing them with traditional orthogonal schemes. Our work provides valuable insights into the potential of NOMA for high-speed V2X communications, and offers a novel contribution to the existing literature by presenting a closed-form expression allowing the development of efficient and reliable 5G V2X systems.

Index Terms—Sensor networks, IoT, 5G, V2X, Non-Orthogonal Multiple Access, Multi-Carrier Modulation, Mobility Channel.

I. INTRODUCTION

The maximum achievable sum rate is a critical question in the design and implementation of future vehicular communication systems, particularly in the context of emerging cellular IoT with massive IoT sensors and devices. It helps determining the overall capacity and efficiency of the system. With a wide range of potential use cases, such as extended sensors, vehicular platooning, remote driving, and video data sharing for automated driving [1], [2], it is important to ensure that the system has the necessary resources to meet the diverse needs of these applications. For example, a high sum rate can improve the reliability and reduce the latency of sensor data transmission, ensuring that critical information is received in real-time. Similarly, a high sum rate can improve the quality and speed of video data sharing, which is essential for autonomous vehicles to make accurate decisions in real-world scenarios.

A variety of technologies have been examined in order to develop solutions that can effectively support the communication needs of vehicles. One such technology is multi-carrier modulation (MCM), which is a digital modulation technique that can support high data rates and is resistant to interference and fading. Another technology is non-orthogonal multiple access (NOMA), which allows multiple users to share the same time-frequency resources and can improve spectral efficiency and coverage. Previous studies have extensively investigated the performance of MCM-NOMA in vehicular systems, focusing on various aspects such as precoding methods [3], rate analysis [4]–[7], resource allocation optimization [6]–[9], and bit error rate analysis [10]–[12] among others.

For instance, in [4], we evaluated the sum rate performance of NOMA combination with different MCM schemes. Works such as [6], [7] have addressed sum rate maximization techniques, but without providing closed-form expressions for the sum rate. Other studies, such as [10]–[12], have focused on bit error rate analysis but without a comprehensive closed-form expression for the sum rate in the general case with n users. Studies such as [6]–[8] have proposed various resource allocation techniques to optimize the performance of MCM-NOMA systems. These techniques aim to allocate power, subcarriers, or time slots among the users to maximize the sum rate or achieve other objectives such as energy efficiency. However, similar to the previous works mentioned, the analysis has either relied on simulation results or lacked a closed-form expression.

In contrast, our work specifically addresses the maximum achievable sum rate of a downlink MCM-NOMA system with n users in a vehicular communication scenario. We derive a closed-form expression for the sum rate, which allows for efficient and reliable analysis without the need for extensive simulations. Our work complements the existing literature by providing valuable insights into the performance of MCM-NOMA systems in high-speed vehicular scenarios and contributes to the development of efficient and reliable 5G V2X systems. Furthermore, we perform a simulation showing the results of our theoretical foundation and compare it with the conventional orthogonal multiple access (OMA) schemes.

The rest of the article is organized as follows: In Section II, the MCM-NOMA system model and problem formulation are introduced. Section III presents the derivation of analytical expressions for the sum rate of a downlink MCM-NOMA system. In Section IV, numerical results are provided for a specific MCM-NOMA system. Finally, conclusions are presented in Section V.

II. SYSTEM MODEL AND PROBLEM FORMULATION

We consider a downlink cellular multi-carrier NOMA system, shown in Fig. 1, wherein a base station communicates with n mobile

Corresponding author: I. Dayoub (e-mail: iyad.dayoub@uphf.fr).
Associate Editor: .
Digital Object Identifier 10.1109/LSENS.2023.0000000

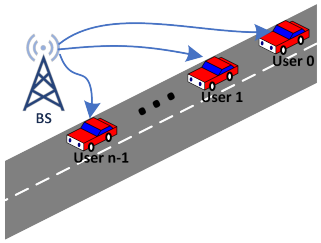

Fig. 1. The system model of a base station transmitting simultaneously to n users using NOMA.

users. A doubly selective fading channel model is adopted due to users' mobility. In a multi-carrier scheme, the transmitted signal is represented by [13]

$$s(t) = \sum_{k=0}^{K-1} \sum_{l=0}^{L-1} g_{l,k}(t) x_{l,k}, \tag{1}$$

where $s(t)$ is the transmitted signal. $x_{l,k}$ is the symbol (message) being transmitted at time-position k and subcarrier-position l. $g_{l,k}$ is the synthesis function which maps $x_{l,k}$ into the signal space. The family of $g_{l,k}(t)$ is referred to as a Gabor system when it is given by Eq. (2).

$$g_{l,k}(t) = p_{tx}(t - kT) \mathrm{e}^{\mathrm{j}2\pi lF(t-kT)} \mathrm{e}^{\mathrm{j}\theta_{l,k}} \tag{2}$$

$p_{tx}(t)$ is the prototype filter (also known as pulse shape, Gabor atom). T is the symbol spacing in time, and F is the subcarrier spacing. Due to the superposition coding required at the transmitter in NOMA, the sent message is written as in Eq. (3).

$$x_{l,k} = \sqrt{P} \sum_{U_i=U_0}^{U_{n-1}} \sqrt{\alpha_{U_i}} * d_{U_i} \tag{3}$$

d_{U_i} is the transmitted symbols to the i^{th} user U_i. α_{U_i} is the power allocation factor of U_i, where $\Sigma_{U_i=U_0}^{U_{n-1}} \alpha_{U_i} = 1$. P is the total base station's transmit power. Without losing generalization, it can be assumed that the weakest user U_0 benefits from the highest power allocation, while the lowest power is given to the strongest user U_{n-1}. Assuming a linear time-varying multipath communication channel $h(\tau, t)$, the received symbol $y_{l,k}$ located on time index k and subcarrier index l is decoded by projecting the received signal $r(t)$ onto the basis pulses (analysis function) $q_{l,k}(t)$.

$$r(t) = \int_{\tau} h(\tau, t) s(t - \tau) \mathrm{d}\tau + \eta(t), \tag{4}$$

$$y_{l,k} = \langle r(t), q_{l,k}(t) \rangle = \int_{-\infty}^{\infty} r(t) q_{l,k}^{*}(t) \mathrm{d}t \tag{5}$$

where $\eta(t)$ is the additive white Gaussian noise (AWGN), and $q_{l,k}$ is given by an equation similar to Eq. (2) as follows

$$q_{l,k}(t) = p_{rx}(t - kT) \mathrm{e}^{\mathrm{j}2\pi lF(t-kT)} \mathrm{e}^{\mathrm{j}\theta_{l,k}} \tag{6}$$

Since the signal is generated in the discrete time domain and to simplify the analytic follow-up in a doubly selective channel, we will use the matrix description and move to the discrete time domain [14]. We write the sampled basis pulse of the synthesis functions $\mathbf{g}_{l,k}(t)$ and $\mathbf{q}_{l,k}(t)$ in a basis pulse vectors $\mathbf{g}_{l,k}$ and $\mathbf{q}_{l,k} \in \mathbb{C}^{N \times 1}$, respectively. By stacking all those basis pulse vectors in transmit and receive matrices $\mathbf{G}$ and $\mathbf{Q} \in \mathbb{C}^{N \times LK}$, respectively. The data and received symbols are also represented in transmit and receive symbol vectors $\mathbf{x}$ and $\mathbf{y} \in \mathbb{C}^{LK \times 1}$, respectively.

$$\mathbf{G} = \begin{bmatrix} \mathbf{g}_{0,0} & \cdots & \mathbf{g}_{L-1,0} & \mathbf{g}_{0,1} & \cdots & \mathbf{g}_{L-1,K-1} \end{bmatrix} \tag{7}$$

$$\mathbf{Q} = \begin{bmatrix} \mathbf{q}_{0,0} & \cdots & \mathbf{q}_{L-1,0} & \mathbf{q}_{0,1} & \cdots & \mathbf{q}_{L-1,K-1} \end{bmatrix} \tag{8}$$

$$\mathbf{x} = \begin{bmatrix} x_{0,0} & \cdots & x_{L-1,0} & x_{0,1} & \cdots & x_{L-1,K-1} \end{bmatrix}^{\mathsf{T}} \tag{9}$$

$$\mathbf{y} = \begin{bmatrix} y_{0,0} & \cdots & y_{L-1,0} & y_{0,1} & \cdots & y_{L-1,K-1} \end{bmatrix}^{\mathsf{T}} \tag{10}$$

Eq. (1) and Eq. (5) can be represented in matrix form as

$$\mathbf{s} = \mathbf{G}\mathbf{x} \tag{11}$$

$$\mathbf{y} = \mathbf{Q}^{\mathsf{H}}\mathbf{r} = \mathbf{Q}^{\mathsf{H}}\mathbf{H}\mathbf{G}\mathbf{x} + \eta \tag{12}$$

where $\mathbf{s}, \mathbf{r} \in \mathbb{C}^{N \times 1}$, $\mathbf{H} \in \mathbb{C}^{N \times N}$, $[\cdot]^H$ is the Hermitian operator, and $\eta \sim \mathcal{CN}(\mathbf{0}, P_\eta) \in \mathbb{C}^{LK \times 1}$ with P_η the white Gaussian noise power in the time domain. By reformulating Eq. (12), the received symbol at subcarrier position l and time position k can be expressed by

$$y_{l,k} = \mathbf{q}_{l,k}^{\mathsf{H}} \mathbf{H} \mathbf{G} \mathbf{x} + \eta_{l,k}, \tag{13}$$

where $\mathbf{y}_{l,k}$ and $\eta_{l,k} \in \mathbb{C}$. The Kronecker "vec trick" property can be used to rewrite this equation

$$y_{l,k} = \underbrace{\left((\mathbf{G}\mathbf{x})^{\mathsf{T}} \otimes \mathbf{q}_{l,k}^{\mathsf{H}} \right) \mathrm{vec}\{\mathbf{H}\}}_{\tilde{y}_{l,k}} + \eta_{l,k}, \tag{14}$$

whereas $\mathrm{vec}\{\cdot\}$ denotes the vectorization operator, $[\cdot]^T$ is the transpose operator, and $\otimes$ represents the Kronecker product.

III. DERIVATION OF THE MAXIMUM SUM RATE

The sum rate, which represents the overall achievable rate for all users, is written as follows:

$$R^{\mathrm{sum}} = \sum_{U_i=U_0}^{U_{n-1}} R^{U_i} \tag{15}$$

$$R^{U_i} = \frac{\gamma}{T} \sum_{j=0}^{LK-1} \log_2 \left(1 + \mathrm{SINR}_j^{U_i} \right) \tag{16}$$

where R^{U_i} express the achieved data rate of i^{th} user U_i, γ is related to the signal constellation. To calculate the Signal to Interference and Noise Ratio (SINR) of the j^{th} symbol, we need to calculate the power of U_i signal $P^{U_i} = |d_{U_i}|^2$, the power of the channel-induced interference (CII) $P_{\mathrm{CII}}^{U_j}$, and the power of the NOMA-induced interference (NII) $P_{\mathrm{NII}}^{U_j}$. At the strongest user U_{n-1} and assuming a perfect SIC, the NII component will be omitted. The SINR can be expressed as:

$$\begin{aligned} \mathrm{SINR}_j^{U_i} &= \frac{P^{U_i}}{P_{\mathrm{CII}}^{U_i} + P_{\mathrm{NII}}^{U_i} + P_\eta}; U_i \in \{U_0, \ldots, U_{n-2}\} \\ \mathrm{SINR}_j^{U_{n-1}} &= \frac{P^{U_{n-1}}}{P_{\mathrm{CII}}^{U_{n-1}} + P_\eta}; U_i = U_{n-1} \end{aligned} \tag{17}$$

Starting from Eq. (14), we can show that

$$P^{U_i} = \alpha_{U_i} [\mathbf{\Gamma}]_{j,j} \tag{18}$$

$$P_{\mathrm{CII}}^{U_i} = \alpha_{U_i} (\mathrm{tr}\{\mathbf{\Gamma}\} - [\mathbf{\Gamma}]_{j,j}) \tag{19}$$

$$P_{\mathrm{NII}}^{U_i} = \sum_{U_j=U_{i+1}}^{U_{n-1}} \alpha_{U_j} \mathrm{tr}\{\mathbf{\Gamma}\} \tag{20}$$

with matrix $\mathbf{\Gamma} = \mathbb{E}\{\tilde{y}_{l,k}\tilde{y}_{l,k}^{\mathsf{H}}\} \in \mathbb{C}^{LK\times LK}$ given by

$$\mathbf{\Gamma} = \left(\mathbf{G}^{\mathsf{T}} \otimes \mathbf{q}_{l,k}^{\mathsf{H}}\right) \mathbf{R}_{\mathrm{vec}\{\mathbf{H}\}} \left(\mathbf{G}^{\mathsf{T}} \otimes \mathbf{q}_{l,k}^{\mathsf{H}}\right)^{\mathsf{H}} \tag{21}$$

where $\mathbf{R}_{\mathrm{vec}\{\mathbf{H}\}} = \mathbb{E}\{\mathrm{vec}\{\mathbf{H}\}\mathrm{vec}\{\mathbf{H}\}^{\mathsf{H}}\} \in \mathbb{C}^{N^2\times N^2}$ is the correlation matrix which depends on the underlying channel model. We can write the SINR in terms of $\mathbf{\Gamma}$ as follows:

$$\begin{aligned} \mathrm{SINR}_j^{U_i} &= \frac{\alpha_{U_i}[\mathbf{\Gamma}]_{j,j}}{\sum_{U_j=U_i}^{U_{n-1}} \left(\alpha_{U_j}\mathrm{tr}\{\mathbf{\Gamma}\}\right) - \alpha_{U_i}[\mathbf{\Gamma}]_{j,j} + P_\eta} \\ \mathrm{SINR}_j^{U_{n-1}} &= \frac{\alpha_{U_{n-1}}[\mathbf{\Gamma}]_{j,j}}{\alpha_{U_{n-1}}(\mathrm{tr}\{\mathbf{\Gamma}\} - [\mathbf{\Gamma}]_{j,j}) + P_\eta} \end{aligned} \tag{22}$$

where $\mathrm{tr}\{\cdot\}$ is the trace of matrix operator, and $j = l + Lk$ represents the j^{th} index of the vectorized symbol.

To the best of our knowledge, due to the complexity of Eq. (21), it is too hard to derive a compact closed-form expression for the sum rate of multicarrier NOMA system in doubly selective channel. However its upper bound can be found by theoretically assuming a doubly flat Rayleigh fading channel.

$$\boldsymbol{H} \;=\; \overline{\boldsymbol{h}}\; \boldsymbol{I_N}, \tag{23}$$

where $\overline{h} \;\sim\; \mathcal{CN}\left(0,\ \sigma^2\right)$, $E(\overline{|h|}^2) = \sigma^2$ and $\boldsymbol{I_N}$ is the identity matrix of size N. With this assumption, we were able, after exhaustive calculation, to write the previous equations in closed-forms in terms of the elements of the basic pulse vectors. As a part of our work to derive a closed-form of $\mathbf{\Gamma}$, we spread the $\mathbf{G}^T \otimes \mathbf{q}_{l,k}^H \in \mathbb{C}^{LK\times N^2}$ part of Eq. (21) as shown in the matrix (24). $\overline{[\cdot]}$ is the complex conjugate of matrix element and

$$\begin{aligned} \boldsymbol{g}_{l,k} &= \begin{bmatrix} [\mathbf{g}_{l,k}]_0 & [\mathbf{g}_{l,k}]_1 & \dots & [\mathbf{g}_{l,k}]_{N-1} \end{bmatrix}^T \\ \boldsymbol{q}_{l,k} &= \begin{bmatrix} [\mathbf{q}_{l,k}]_0 & [\mathbf{q}_{l,k}]_1 & \dots & [\mathbf{q}_{l,k}]_{N-1} \end{bmatrix}^T \end{aligned}$$

With the matrix (24), we can derive a closed-form formula for the diagonal elements of Eq. (21) in the case of a doubly flat Rayleigh fading channel as

$$[\mathbf{\Gamma}]_{j,j} = \sigma^2 \sum_{i=0}^{N-1} \left[\boldsymbol{g}_{u,v}\right]_i \overline{[\boldsymbol{q}_{l,k}]_i} \sum_{i=0}^{N-1} \overline{\left[\boldsymbol{g}_{u,v}\right]_i\ \overline{[\boldsymbol{q}_{l,k}]_i}} \tag{25}$$

where u and v are the integer remainder and quotient of j divided by L, respectively. We can express the trace of the matrix $\mathbf{\Gamma}$ as

$$\mathrm{tr}\{\mathbf{\Gamma}\} = \sigma^2 \sum_{m=0}^{LK-1} \left(\sum_{i=0}^{N-1} \left[\boldsymbol{g}_{u,v}\right]_i \overline{[\boldsymbol{q}_{l,k}]_i} \sum_{i=0}^{N-1} \overline{\left[\boldsymbol{g}_{u,v}\right]_i\ \overline{[\boldsymbol{q}_{l,k}]_i}} \right) \tag{26}$$

The SINR in (22) can be reformulated for a doubly flat Rayleigh fading channel using Eq. (25) and (26). The maximum achievable sum rate for an n user MCM-NOMA system can be expressed as in Eq. (27). This equation shows that the upper-bound of the sum rate depends namely on NOMA power allocation factors and MCM basis pulse of the synthesis functions α_{U_i}, $g_{u,v}$ and $q_{l,k}$. Hence Eq. (27) can be used as a reference for understanding the factors that affect the performance of MCM-NOMA systems.

IV. RESULTS

In this section, we perform numerical simulations of the studied system model. A Cyclic Prefix – Orthogonal Frequency Division Multiplexing (CP-OFDM) is adopted as a multi-carrier modulation method. Wherein three users (User 0, 1, and 2) are communicating with a base station in OFDM-based NOMA and OMA schemes. This is done for a given carrier frequency of 2.5 GHz and a subcarrier spacing of 15 kHz. Regarding the OFDM design parameters, 300 subcarriers, 14 OFDM symbols in time, time-frequency spacing of $TF = 1.07$, a sinc pulse filter, and a 4 Quadrature Amplitude Modulation (QAM) signal constellation are adopted. We consider a NOMA power allocation factor of $\alpha_{U_0} = 0.8$, $\alpha_{U_1} = 0.15$, $\alpha_{U_2} = 0.05$ based on the results of a previous study [15], and a doubly selective channel with Vehicular A power delay profile and Jakes Doppler model. The Vehicular A power delay profile describes the distribution of signal power over different delay components in vehicular environments [16], while the Jakes Doppler model is a standard model for studying the impact of multipath fading caused by the relative motion between the transmitter and receiver [17].

Fig. 2a compares the sum rates of OFDM-NOMA and their corresponding OFDM-OMA in doubly flat/selective channels, with users' speeds of $v_0 = 90$, $v_1 = 110$, and $v_2 = 130$ km/h. The results clearly indicate that OFDM-NOMA achieves significant power savings, with a remarkable 10 dB gap between NOMA and OMA for the same sum rate, as depicted in Fig. 2a. According to the requirements of 5G V2X use cases [1], our obtained results meet the minimum data rate requirements at the smallest/most used subcarrier frequency spacing of 15 kHz. Furthermore, they can also fulfill the maximum data rate requirements when selecting a larger subcarrier frequency, such as 240 kHz.

Fig. 2b and 2c illustrate the impact of user mobility on the sum rate of OFDM-NOMA and OFDM-OMA, at a fixed SNR of 25

$$\mathbf{G}^T \otimes \mathbf{q}_{l,k}^H = \begin{bmatrix} [\mathbf{g}_{0,0}]_0\overline{[\mathbf{q}_{l,k}]_0} & \cdots & [\mathbf{g}_{0,0}]_0\overline{[\mathbf{q}_{l,k}]_{N-1}} & [\mathbf{g}_{0,0}]_1\overline{[\mathbf{q}_{l,k}]_0} & \cdots & [\mathbf{g}_{0,0}]_{N-1}\overline{[\mathbf{q}_{l,k}]_{N-1}} \\ \vdots & \ddots & \vdots & \vdots & \ddots & \vdots \\ [\mathbf{g}_{L-1,0}]_0\overline{[\mathbf{q}_{l,k}]_0} & \cdots & [\mathbf{g}_{L-1,0}]_0\overline{[\mathbf{q}_{l,k}]_{N-1}} & [\mathbf{g}_{L-1,0}]_1\overline{[\mathbf{q}_{l,k}]_0} & \cdots & [\mathbf{g}_{L-1,0}]_{N-1}\overline{[\mathbf{q}_{l,k}]_{N-1}} \\ [\mathbf{g}_{0,1}]_0\overline{[\mathbf{q}_{l,k}]_0} & \cdots & [\mathbf{g}_{0,1}]_0\overline{[\mathbf{q}_{l,k}]_{N-1}} & [\mathbf{g}_{0,1}]_1\overline{[\mathbf{q}_{l,k}]_0} & \cdots & [\mathbf{g}_{0,1}]_{N-1}\overline{[\mathbf{q}_{l,k}]_{N-1}} \\ \vdots & \ddots & \vdots & \vdots & \ddots & \vdots \\ [\mathbf{g}_{L-1,K-1}]_0\overline{[\mathbf{q}_{l,k}]_0} & \cdots & [\mathbf{g}_{L-1,K-1}]_0\overline{[\mathbf{q}_{l,k}]_{N-1}} & [\mathbf{g}_{L-1,K-1}]_1\overline{[\mathbf{q}_{l,k}]_0} & \cdots & \left[\mathbf{g}_{L-1,K-1}\right]_{N-1}\overline{[\mathbf{q}_{l,k}]_{N-1}} \end{bmatrix} \tag{24}$$

$$\begin{aligned} \mathrm{R}^{\mathrm{sum}} = \frac{\gamma}{T} \sum_{U_i=U_0}^{U_{n-2}} \sum_{j=0}^{LK-1} \log_2 \left(1 + \frac{\alpha_{U_i}\sigma^2 \sum_{i=0}^{N-1}[\boldsymbol{g}_{u,v}]_i\overline{[\boldsymbol{q}_{l,k}]_i} \sum_{i=0}^{N-1}\overline{[\boldsymbol{g}_{u,v}]_i\ \overline{[\boldsymbol{q}_{l,k}]_i}}}{\sum_{U_j=U_i}^{U_{n-1}} \left[\alpha_{U_j}\sigma^2 \sum_{m=0}^{LK-1} \left(\sum_{i=0}^{N-1}[\boldsymbol{g}_{u,v}]_i\overline{[\boldsymbol{q}_{l,k}]_i} \sum_{i=0}^{N-1}\overline{[\boldsymbol{g}_{u,v}]_i\ \overline{[\boldsymbol{q}_{l,k}]_i}} \right)\right] - \alpha_{U_i}\sigma^2 \sum_{i=0}^{N-1}[\boldsymbol{g}_{u,v}]_i\overline{[\boldsymbol{q}_{l,k}]_i} \sum_{i=0}^{N-1}\overline{[\boldsymbol{g}_{u,v}]_i\ \overline{[\boldsymbol{q}_{l,k}]_i}} + P_\eta} \right) \\ + \frac{\gamma}{T} \sum_{j=0}^{LK-1} \log_2 \left(1 + \frac{\alpha_{U_{n-1}}\sigma^2 \sum_{i=0}^{N-1}[\boldsymbol{g}_{u,v}]_i\overline{[\boldsymbol{q}_{l,k}]_i} \sum_{i=0}^{N-1}\overline{[\boldsymbol{g}_{u,v}]_i\ \overline{[\boldsymbol{q}_{l,k}]_i}}}{\alpha_{U_{n-1}}\sigma^2 \sum_{\substack{m=0 \\ m\neq j}}^{LK-1} \left(\sum_{i=0}^{N-1}[\boldsymbol{g}_{u,v}]_i\overline{[\boldsymbol{q}_{l,k}]_i} \sum_{i=0}^{N-1}\overline{[\boldsymbol{g}_{u,v}]_i\ \overline{[\boldsymbol{q}_{l,k}]_i}} \right) + P_\eta} \right) \end{aligned} \tag{27}$$

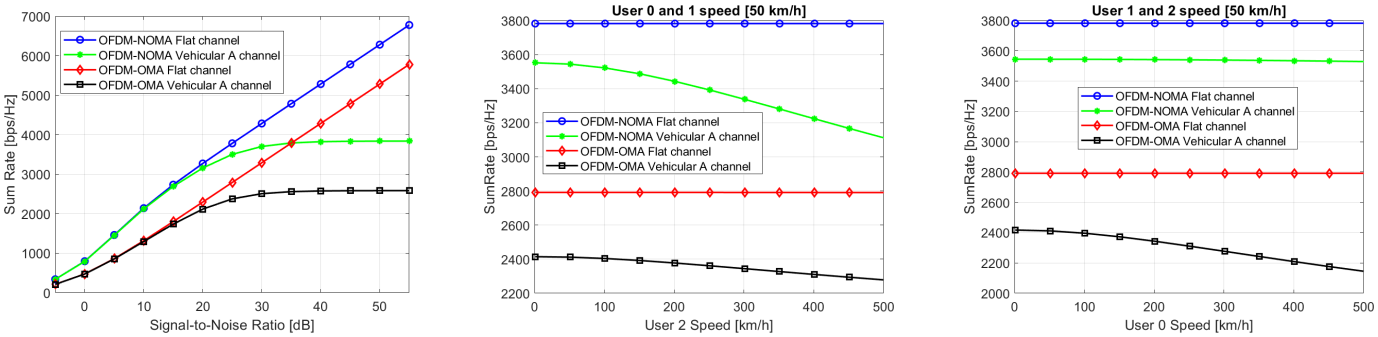

(a) (b) (c)

Fig. 2. (a) Sum rate vs SNR with different power delay profiles. (b) Sum rate over User 2 speed. (c) Sum rate over User 0 speed.

dB. To obtain these results, we varied the speed of the nearest and farthest users with respect to the base station from 0 to 500 km/h, while keeping the speed of the other two users fixed at 50 km/h. As shown in Fig. 2b, OFDM-OMA is less affected by changes in the nearest user's speed than OFDM-NOMA. However, despite this advantage, the sum rate of OFDM-NOMA remains consistently higher, demonstrating the overall superiority of NOMA designs over OMA in achieving higher data rates.

Similarly, Fig. 2c illustrates the impact of user mobility on the sum rate of OFDM-NOMA and OFDM-OMA, but with a focus on the farthest user (User 0) with poorer channel conditions. The findings reveal that OFDM-NOMA exhibits greater resistance to variations in User 0's speed compared to OFDM-OMA. As before, NOMA maintains higher sum rates across different speeds. Interestingly, OFDM-OMA maintains almost the same level of resistance to speed changes, regardless of which user is affected (User 0 or User 2).

The results demonstrate that NOMA exhibits greater resilience to mobility changes of the far user compared to OMA, while OMA's sensitivity to changes in mobility of both near and far users is roughly equivalent. This phenomenon can be explained by considering Eq. (17), which indicates that NOMA-induced interference dominates over channel-induced interference, and the former is ignored when calculating the SINR of User 2. The higher robustness of NOMA to the mobility of the far user can be attributed to the power allocation factor, which assigns a higher power level to the weaker user to overcome its weaker channel conditions. In contrast, in OMA, the transmit power is equally divided among users, which leads to a lower sum rate when one user has a weaker channel.

V. CONCLUSION

In this letter, we derived a closed-form expression for the maximum achievable sum rate of multi-carrier NOMA in a V2X network. This provides a theoretical foundation that can serve as an upper-bound reference for MCM-NOMA solutions, including techniques for optimizing resource allocation and maximizing total data transmission rates. Our theoretical findings have been verified through simulation results. In future work, our theoretical foundation can be extended to consider more complex scenarios such as heterogeneous networks with different channel models, various user distributions, and different mobility models. Moreover, the investigated MCM-NOMA scheme can be combined with other techniques, such as beamforming, to further improve the system's performance.

REFERENCES

[1] A. Alalewi, I. Dayoub, and S. Cherkaoui, "On 5G-V2X Use Cases and Enabling Technologies: A Comprehensive Survey," *IEEE Access*, vol. 9, pp. 107 710–107 737, 2021.

[2] S. Gyawali, S. Xu, Y. Qian, and R. Q. Hu, "Challenges and Solutions for Cellular Based V2X Communications," *IEEE Communications Surveys & Tutorials*, vol. 23, no. 1, pp. 222–255, 2021.

[3] H. Mathur and T. Deepa, "A novel precoded digitized OFDM based NOMA system for future wireless communication," *Optik*, vol. 259, p. 168948, Jun. 2022.

[4] Y. Alsaba, M. Saideh, I. Dayoub, and M. Berbineau, "On the Sum Rate of MCM-Based NOMA and MCM-Based OMA Systems," in *2020 14th International Conference on Signal Processing and Communication Systems (ICSPCS)*, Dec. 2020, pp. 1–5.

[5] N. Jaiswal and N. Purohit, "Performance Analysis of NOMA-Enabled Vehicular Communication Systems With Transmit Antenna Selection Over Double Nakagami-m Fading," *IEEE Transactions on Vehicular Technology*, vol. 70, no. 12, pp. 12 725–12 741, Dec. 2021.

[6] H. Al-Obiedollah, K. Cumanan, H. B. Salameh, G. Chen, Z. Ding, and O. A. Dobre, "Downlink Multi-Carrier NOMA With Opportunistic Bandwidth Allocations," *IEEE Wireless Communications Letters*, vol. 10, no. 11, pp. 2426–2429, Nov. 2021.

[7] Y. Fu, L. Salaün, C. W. Sung, and C. S. Chen, "Subcarrier and Power Allocation for the Downlink of Multicarrier NOMA Systems," *IEEE Transactions on Vehicular Technology*, vol. 67, no. 12, pp. 11 833–11 847, Dec. 2018.

[8] A. J. Muhammed, Z. Ma, P. D. Diamantoulakis, L. Li, and G. K. Karagiannidis, "Energy-Efficient Resource Allocation in Multicarrier NOMA Systems With Fairness," *IEEE Transactions on Communications*, vol. 67, no. 12, pp. 8639–8654, Dec. 2019.

[9] W. Ni, X. Liu, Y. Liu, H. Tian, and Y. Chen, "Resource Allocation for Multi-Cell IRS-Aided NOMA Networks," *IEEE Transactions on Wireless Communications*, vol. 20, no. 7, pp. 4253–4268, Jul. 2021, conference Name: IEEE Transactions on Wireless Communications.

[10] A. A. Hamza, I. Dayoub, I. Alouani, and A. Amrouche, "Enabling User Relaying in MCM-NOMA Under Doubly Selective Channels Using Iterative Interference Cancellation Schemes for Wireless IoT Networks," *IEEE Sensors Letters*, vol. 6, no. 3, pp. 1–4, Mar. 2022.

[11] A. Hilario-Tacuri, J. Maldonado, M. Revollo, and H. Chambi, "Bit Error Rate Analysis of NOMA-OFDM in 5G Systems With Non-Linear HPA With Memory," *IEEE Access*, vol. 9, pp. 83 709–83 717, 2021.

[12] A. A. Hamza, I. Dayoub, I. Alouani, and A. Amrouche, "On the Error Rate Performance of Full-Duplex Cooperative NOMA in Wireless Networks," *IEEE Transactions on Communications*, vol. 70, no. 3, pp. 1742–1758, Mar. 2022.

[13] A. Sahin, I. Guvenc, and H. Arslan, "A Survey on Multicarrier Communications: Prototype Filters, Lattice Structures, and Implementation Aspects," *IEEE Communications Surveys Tutorials*, vol. 16, no. 3, pp. 1312–1338, 2014.

[14] R. Nissel, S. Schwarz, and M. Rupp, "Filter Bank Multicarrier Modulation Schemes for Future Mobile Communications," *IEEE Journal on Selected Areas in Communications*, vol. 35, no. 8, pp. 1768–1782, Aug. 2017.

[15] F. KARA and H. KAYA, "A True Power Allocation Constraint for Non-Orthogonal Multiple Access with M-QAM Signalling," in *2020 IEEE Microwave Theory and Techniques in Wireless Communications (MTTW)*, vol. 1, Oct. 2020, pp. 7–12.

[16] R. Srinivasan, "IEEE 802.16m Evaluation Methodology Document (EMD)," Jul. 2008.

[17] W. C. Jakes, *Microwave mobile communications*. New York: Wiley, 1974.